Binding studies of metal-salphen and metal-bipyridine complexes towards G-quadruplex DNA

Anna Łęczkowska, Jorge Gonzalez-Garcia, Cristina Perez-Arnaiz, Begoña Garcia, Andrew J. P. White, Ramon Vilar[1*]

(a)

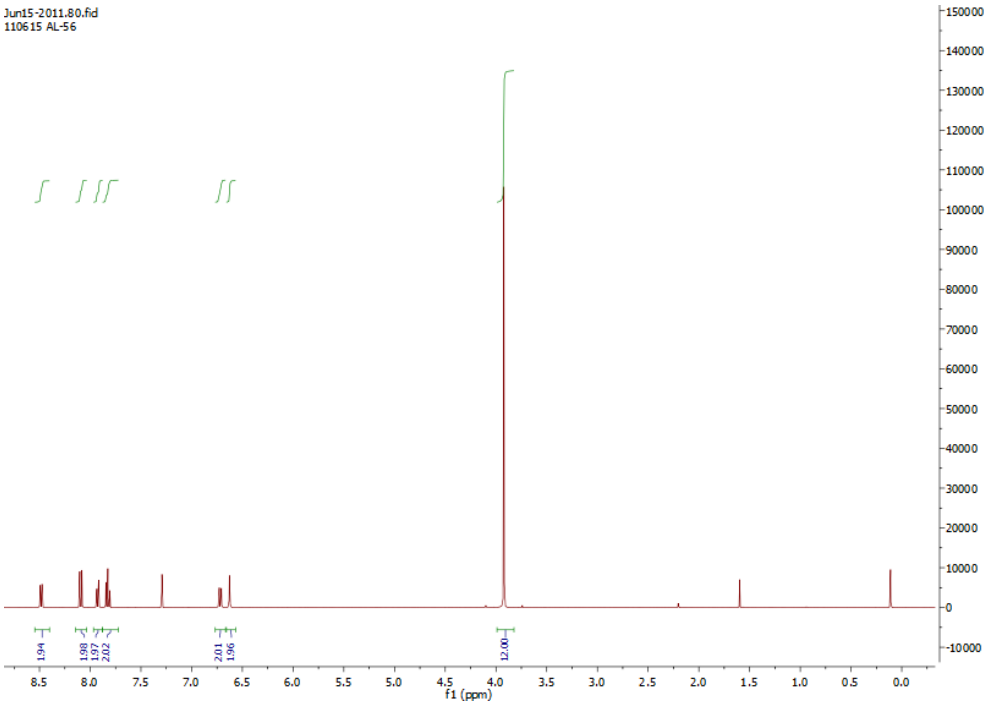

(b)

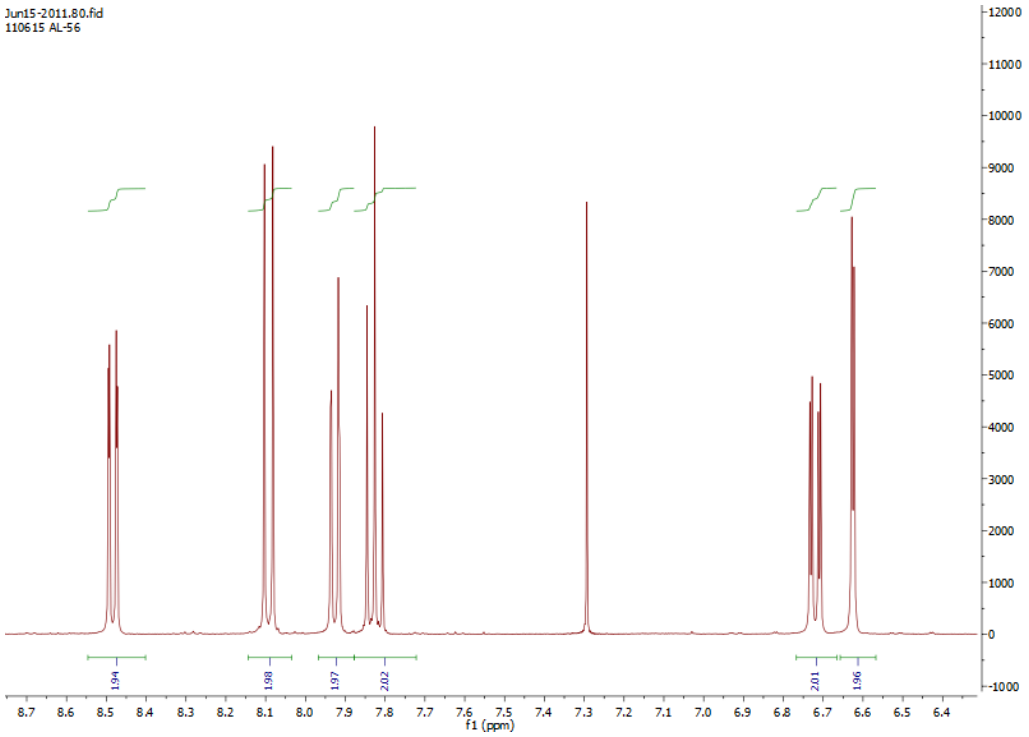

Figure S1. (a) ^{1}H NMR spectrum of compound **6** recorded in $CDCl_3$; (b) zoom-in of the aromatic region of the ^{1}H NMR spectrum of compound **6**

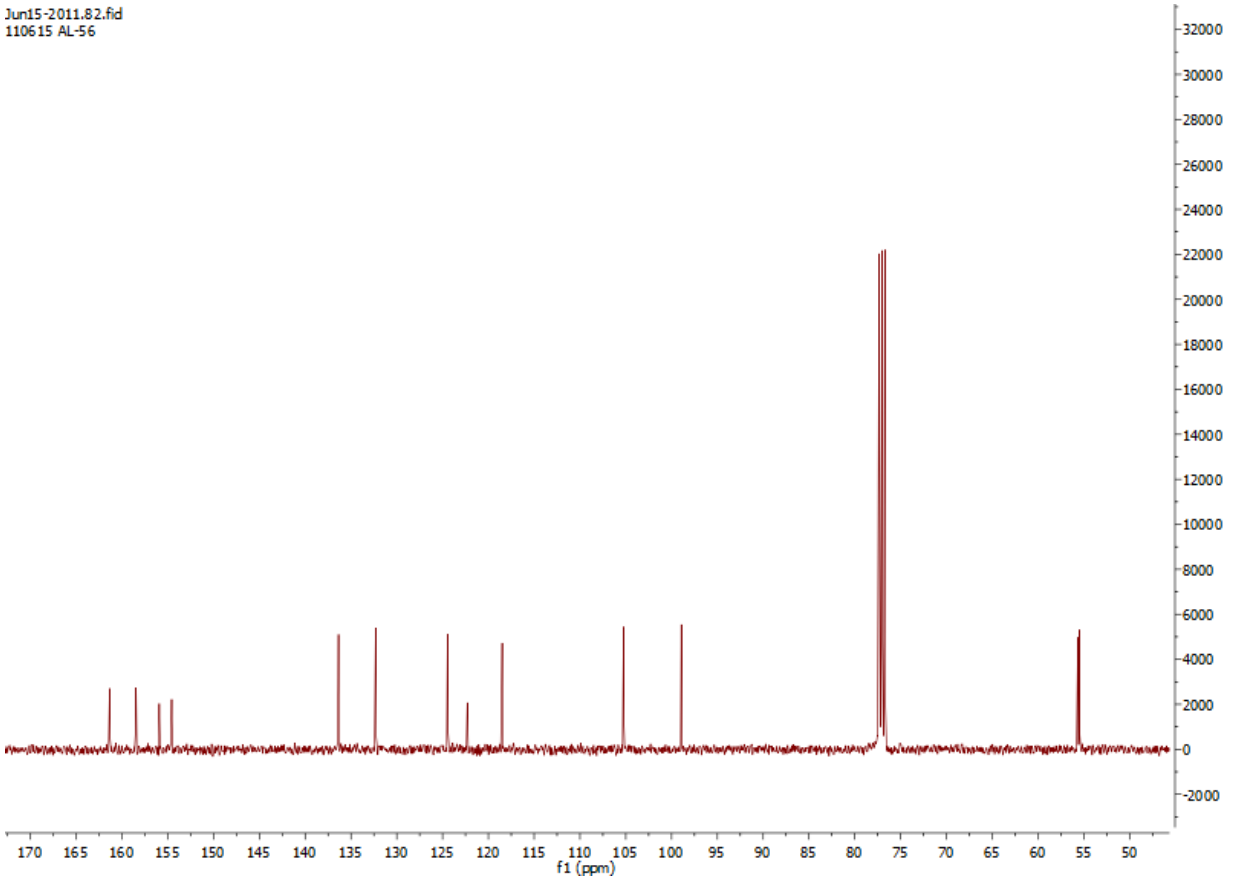

Figure S2. ^{13}C NMR spectrum of bipyridine compound **6** recorded in $CDCl_3$

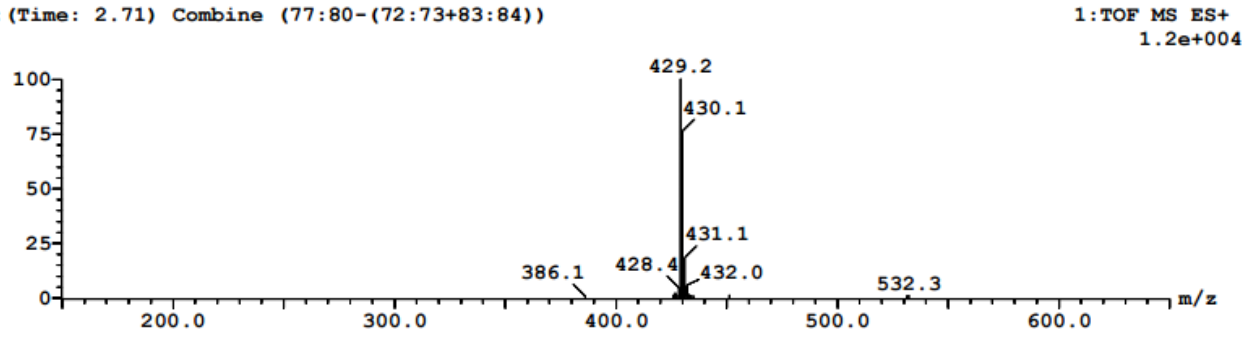

Figure S3. Mass spectrum of compound **6**

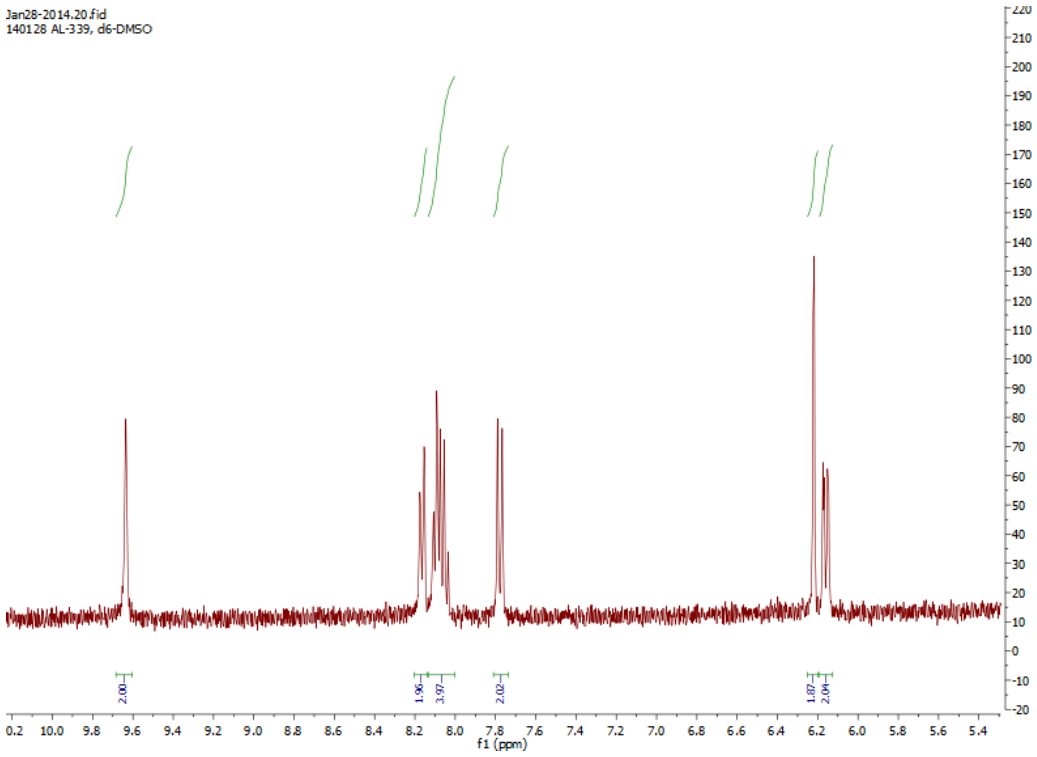

Figure S4. ^{1}H NMR spectrum of complex **8** in d^{6}-DMSO

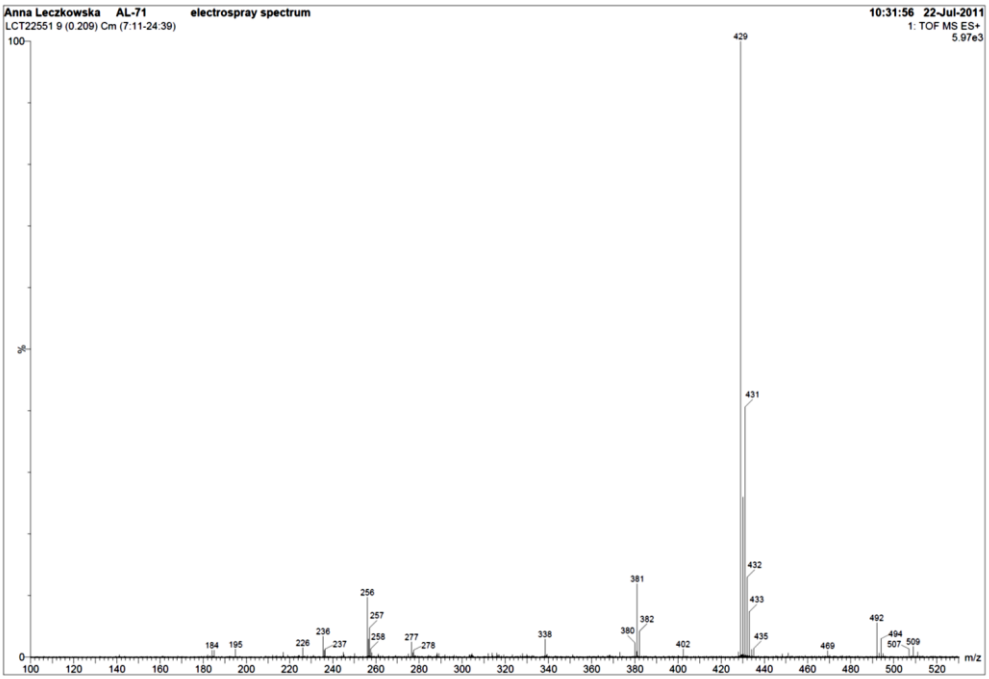

Figure S5. Mass spectrum of complex **8**

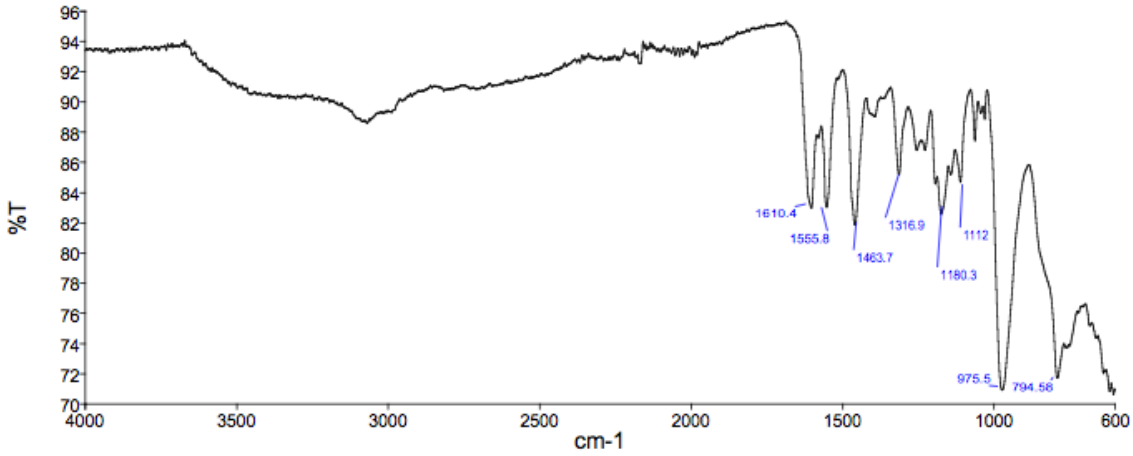

Figure S6. IR spectrum of complex **9**

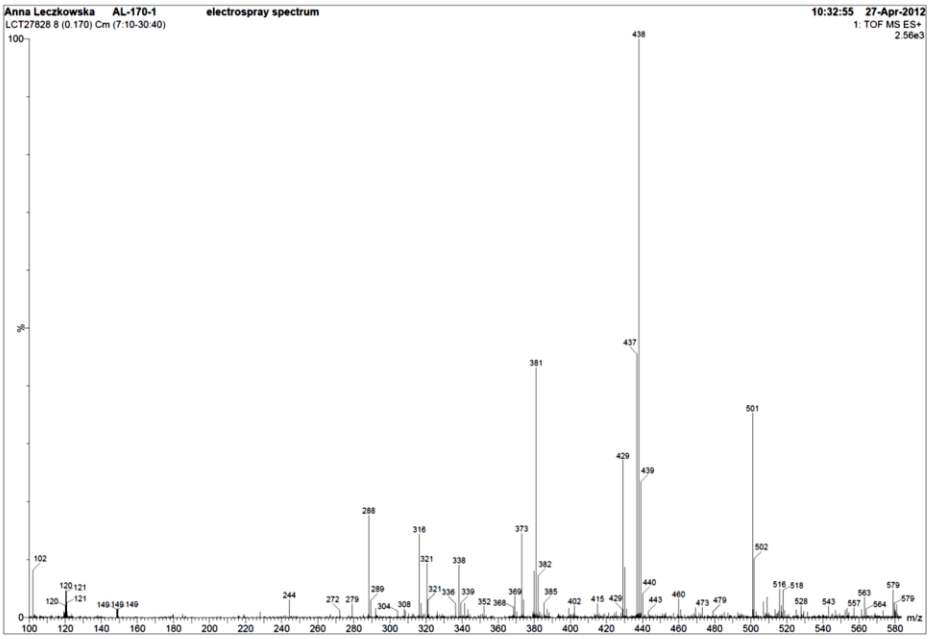

Figure S7. Mass spectrum of complex **9**

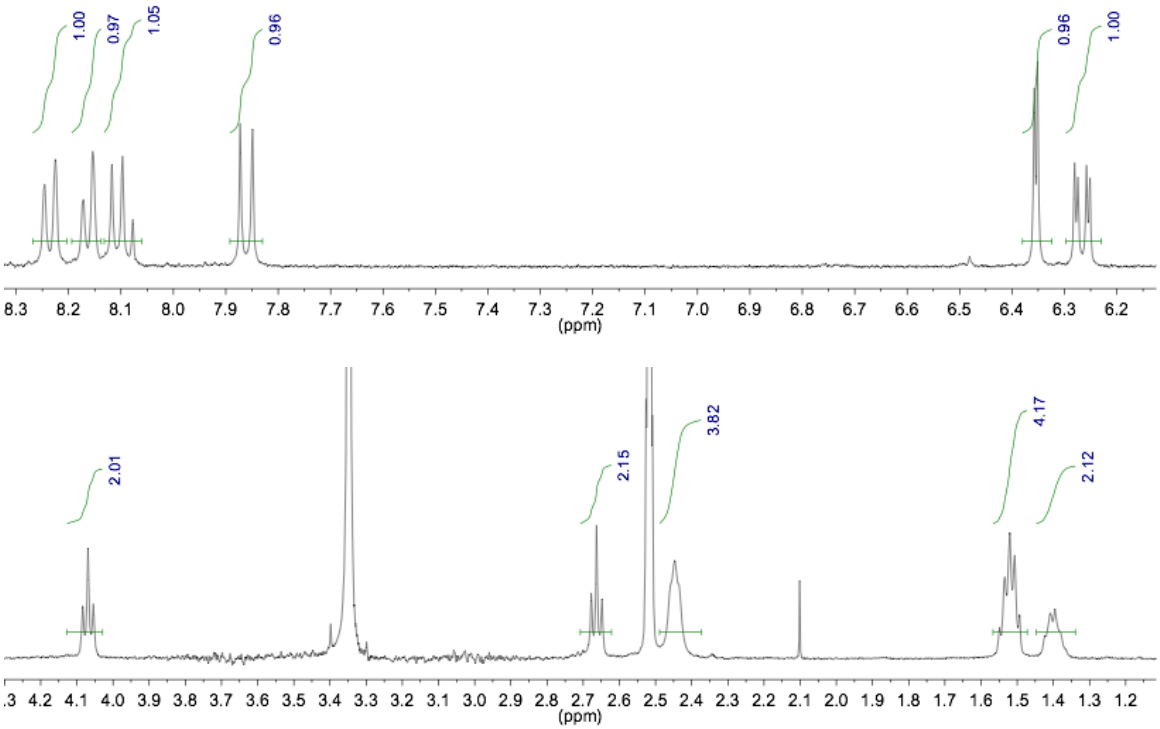

Figure S8. ^{1}H NMR spectrum of complex **4** recorded in d_6-DMSO

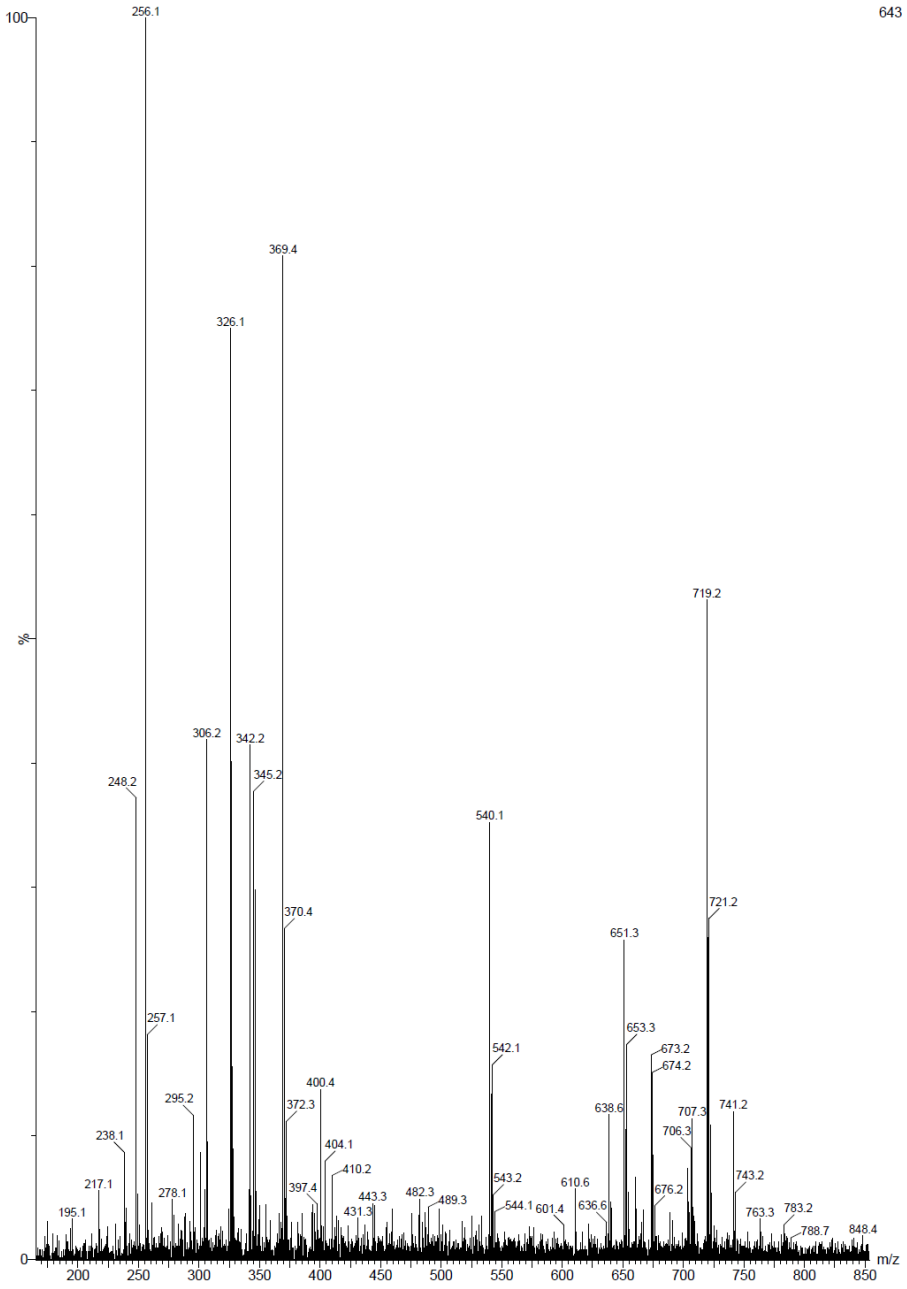

Figure S9. Mass spectrum of complex **4**

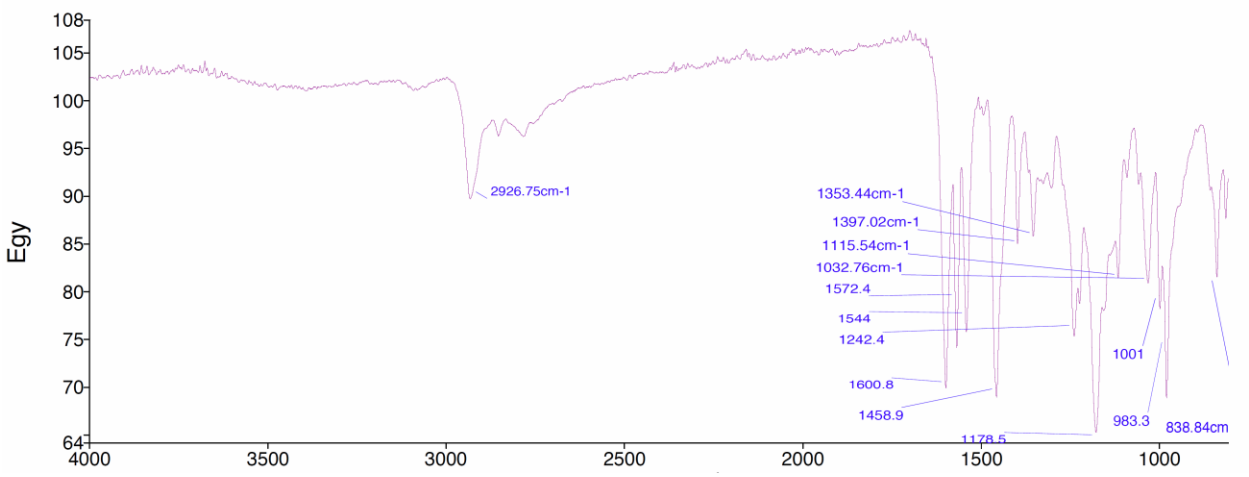

Figure S10. IR spectrum of complex **5**

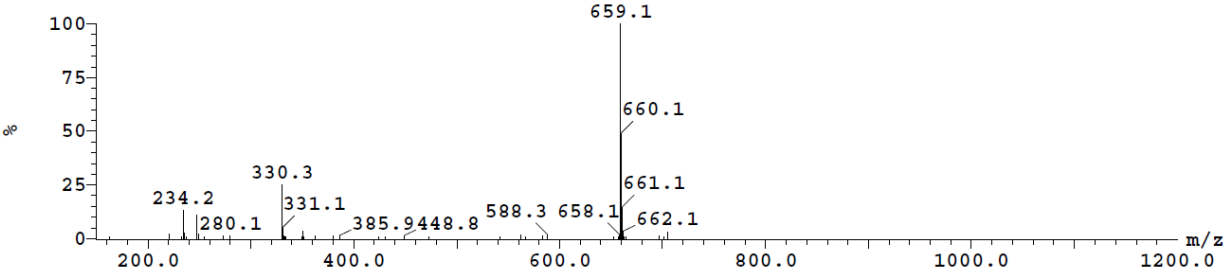

Figure S11. Mass spectrum of complex **5**

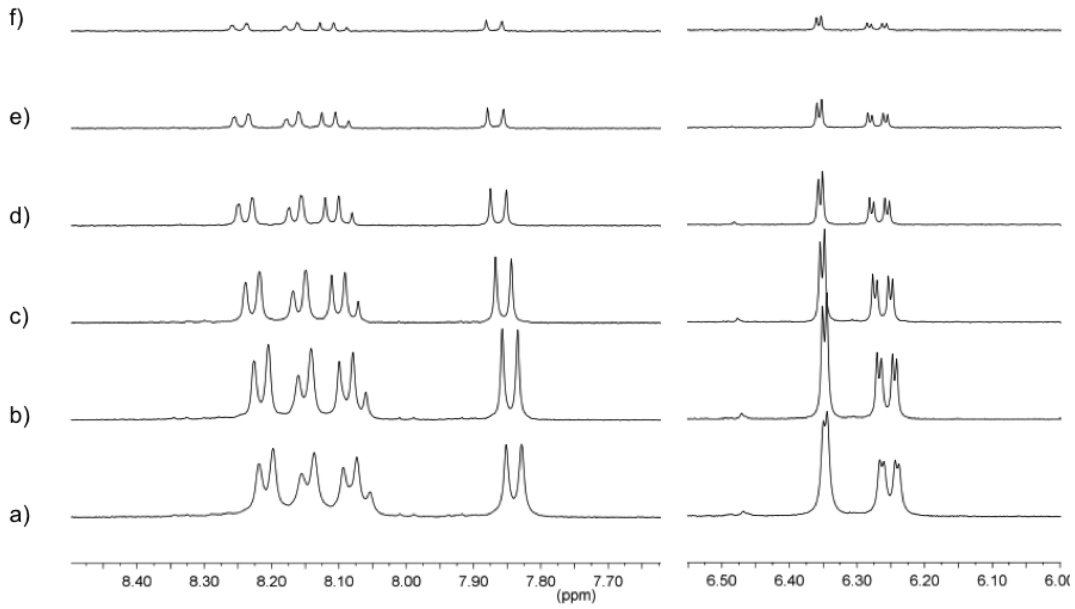

Figure S12. Aromatic region of the ^{1}H NMR spectrum of complex **4** recorded in d_6-DMSO at 20 ^{o}C; a) 15 mM, b) 10 mM, c) 5 mM, d) 2.5 mM, e) 1.25 mM, f) 0.625 mM

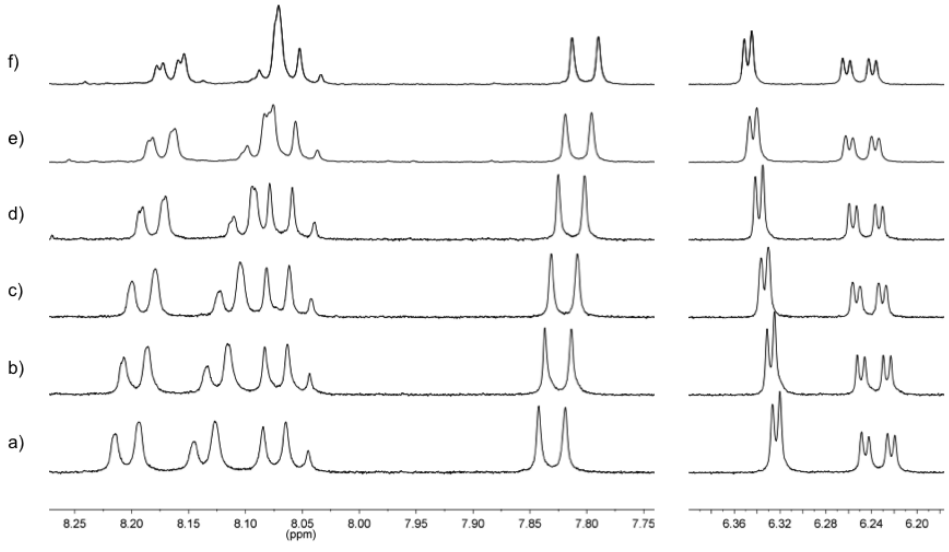

Figure S13. Aromatic region of ^{1}H NMR spectra of complex **4** (5 mM) recorded in d_6-DMSO at: a) 20 ^{o}C , b) 30 ^{o}C , c) 40 ^{o}C , d) 50 ^{o}C , e) 60 ^{o}C f) 70 ^{o}C.

The X-ray crystal structure of 4

The most notable feature of the structure of **4** is the presence of two relatively large residual electron density peaks in chemically meaningless positions as shown in Fig. S2 (the five largest residual electron density peaks are 1.64, 1.58, 0.51, 0.24 and 0.23 eÅ^{-3}). The most obvious explanation would be some unresolved twinning, but careful inspection of the original diffraction data does not support this possibility. Since the peaks do not make any chemical sense, and there does not seem to be any crystallographic reason for them, we have no satisfactory explanation for their presence.

The six hydrogen atoms of the three included water molecules were all located from Δ*F* maps and refined freely subject to an O–H distance constraint of 0.90 Å.

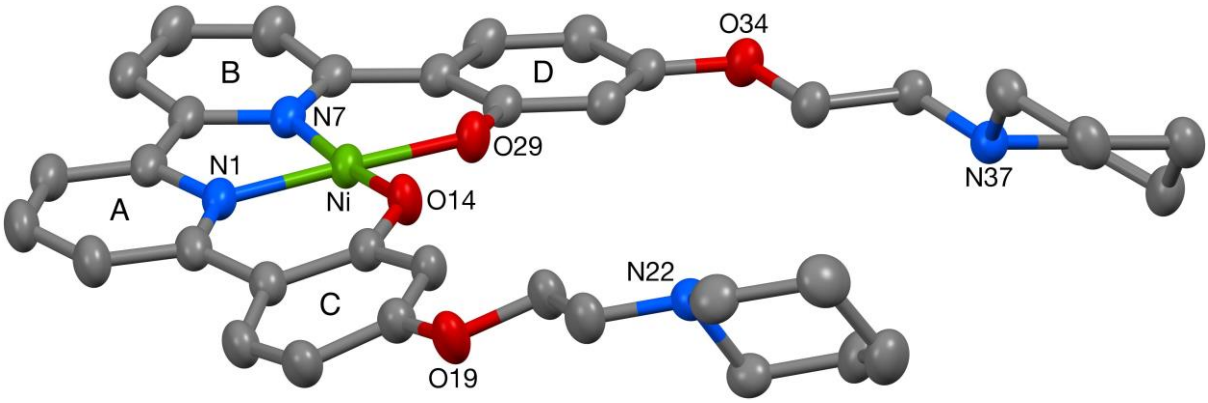

Fig. S14 The crystal structure of **4** (50% probability ellipsoids).

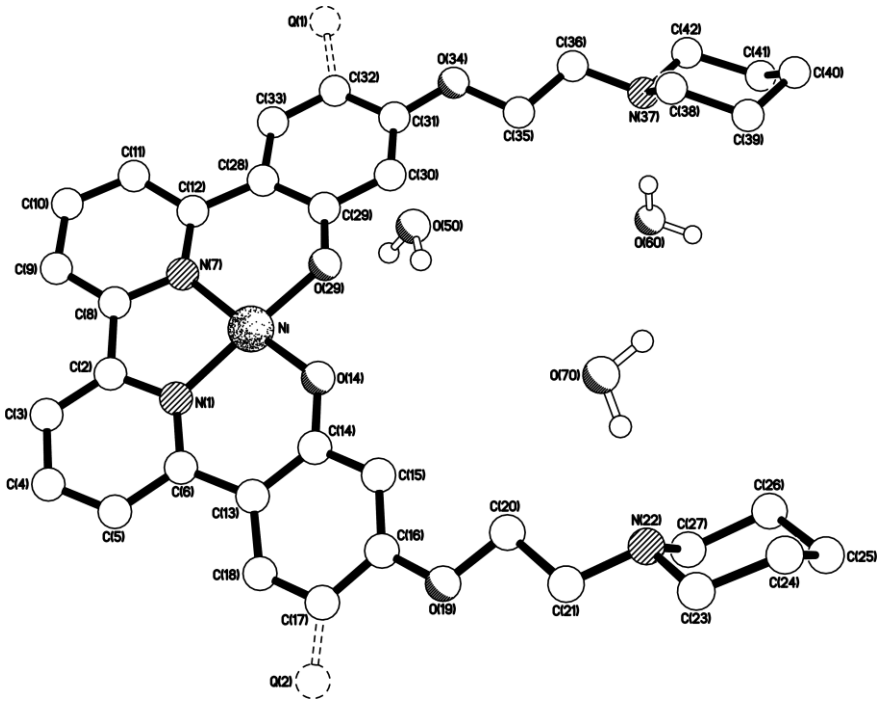

Fig. S15 The crystal structure of **4** showing the positions of the two largest residual electron density peaks, labelled Q(1) and Q(2).

The X-ray crystal structure of 5

The C35-bound -CH_2-$C_5H_{10}N$ arm in the structure of **5** was found to be disordered. Two orientations were identified of *ca*. 63 and 37% occupancy, their geometries were optimised, the thermal parameters of adjacent atoms were restrained to be similar, and only the non-hydrogen atoms of the major occupancy orientation were refined anisotropically (those of the minor occupancy orientation were refined isotropically).

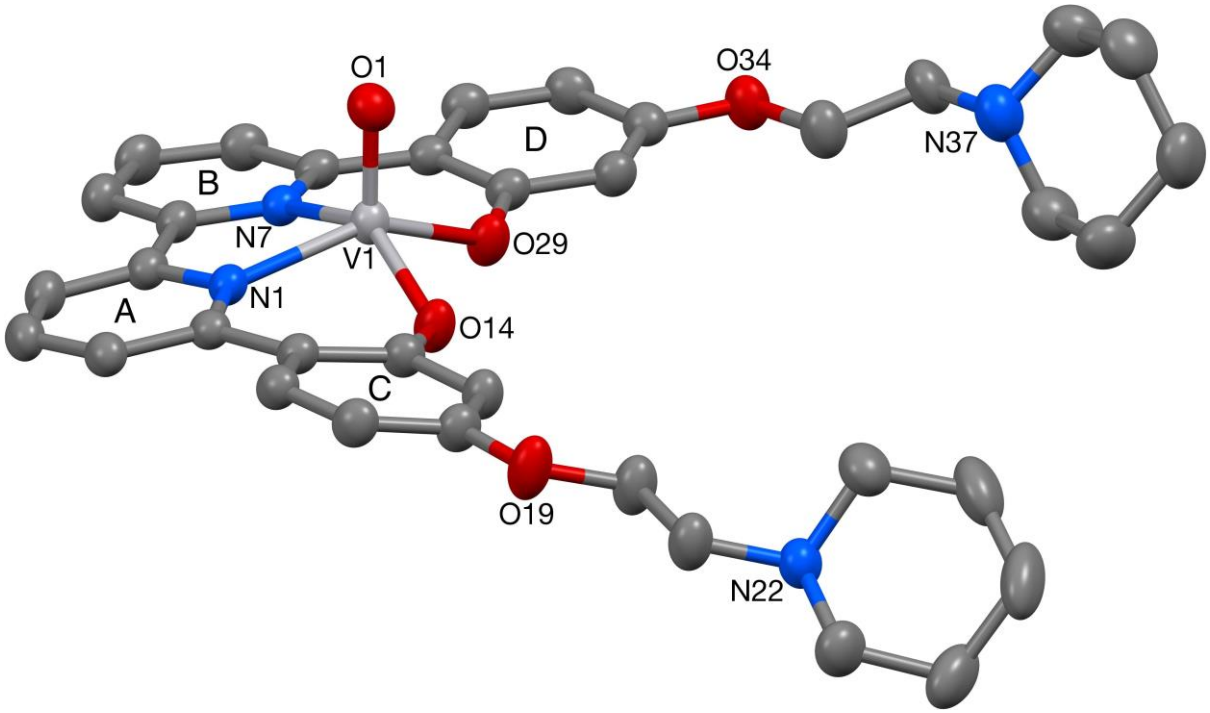

Fig. S16 The crystal structure of **5** (50% probability ellipsoids).

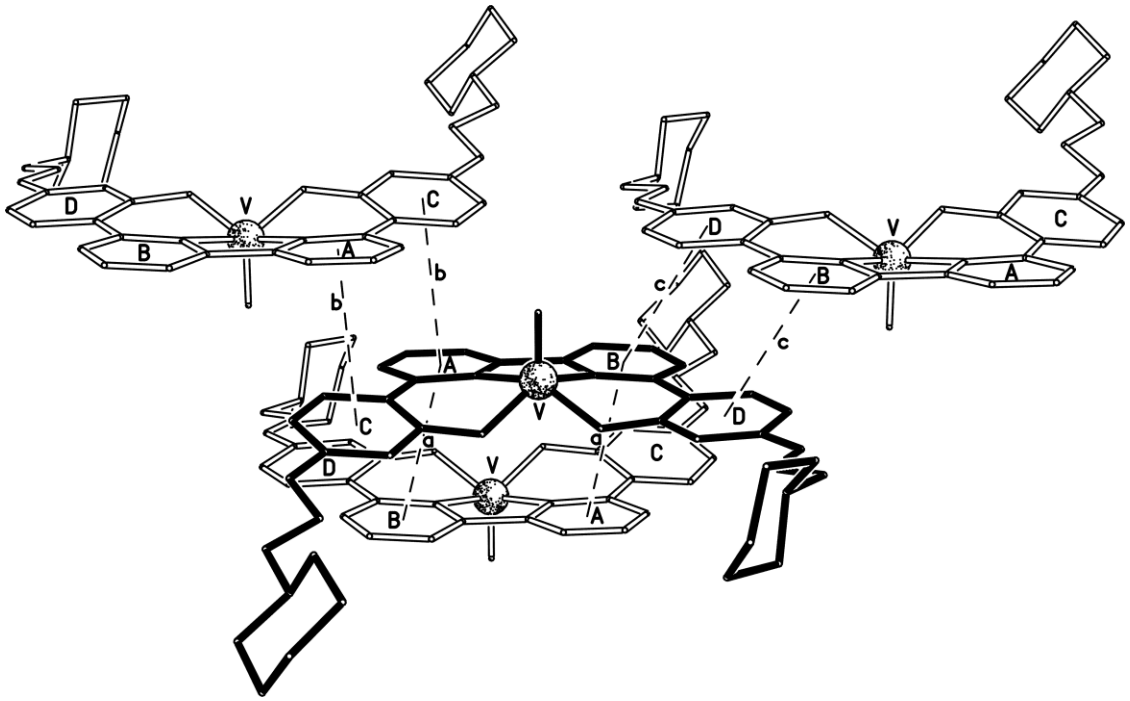

Fig. S17 The π-π packing interactions surrounding one molecule (drawn with dark bonds) in the crystal structure of **5**. Interactions **a**, **b**, and **c** have centroid···centroid and mean interplanar separations (Å) of *ca*. **a**) 3.61 and 3.32, **b**) 3.83 and 3.43, and **c**) 3.93 and 3.39, the ring pairs being inclined by *ca*. 4, 16 and 8° respectively.

Table S1. ΔT_m values determined by FRET melting assays for the different compounds (1 μM) against several DNA structures. Measurements were performed in triplicate.

Compound	ds26	HTelo21	22CTA	c-kit2	26CEB	c-myc	Bcl-2
1	2.5 ± 0.1	20 ± 1	18.2 ± 0.1	14.6 ± 0.2	9.9 ± 0.1	7 ± 3	7.3 ± 0.9
2	3.7 ± 0.1	27 ± 1	20.0 ± 0.9	13.6 ± 0.9	9.4 ± 0.2	12.6 ± 0.5	15.2 ± 0.9
3	3.3 ± 0.1	24.1 ± 0.2	6.0 ± 0.3	15.3 ± 0.1	10.5 ± 0.8	9.9 ± 0.1	13.5 ± 0.2
4	10.3 ± 0.1	37 ± 4	34 ± 3	22 ± 1	17.5 ± 0.5	13.8 ± 0.2	18.3 ± 0.4
5	3.7 ± 0.4	28.2 ± 0.1	19.4 ± 0.1	20.1 ± 0.6	28.8 ± 0.7	10.9 ± 0.1	18.6 ± 0.3

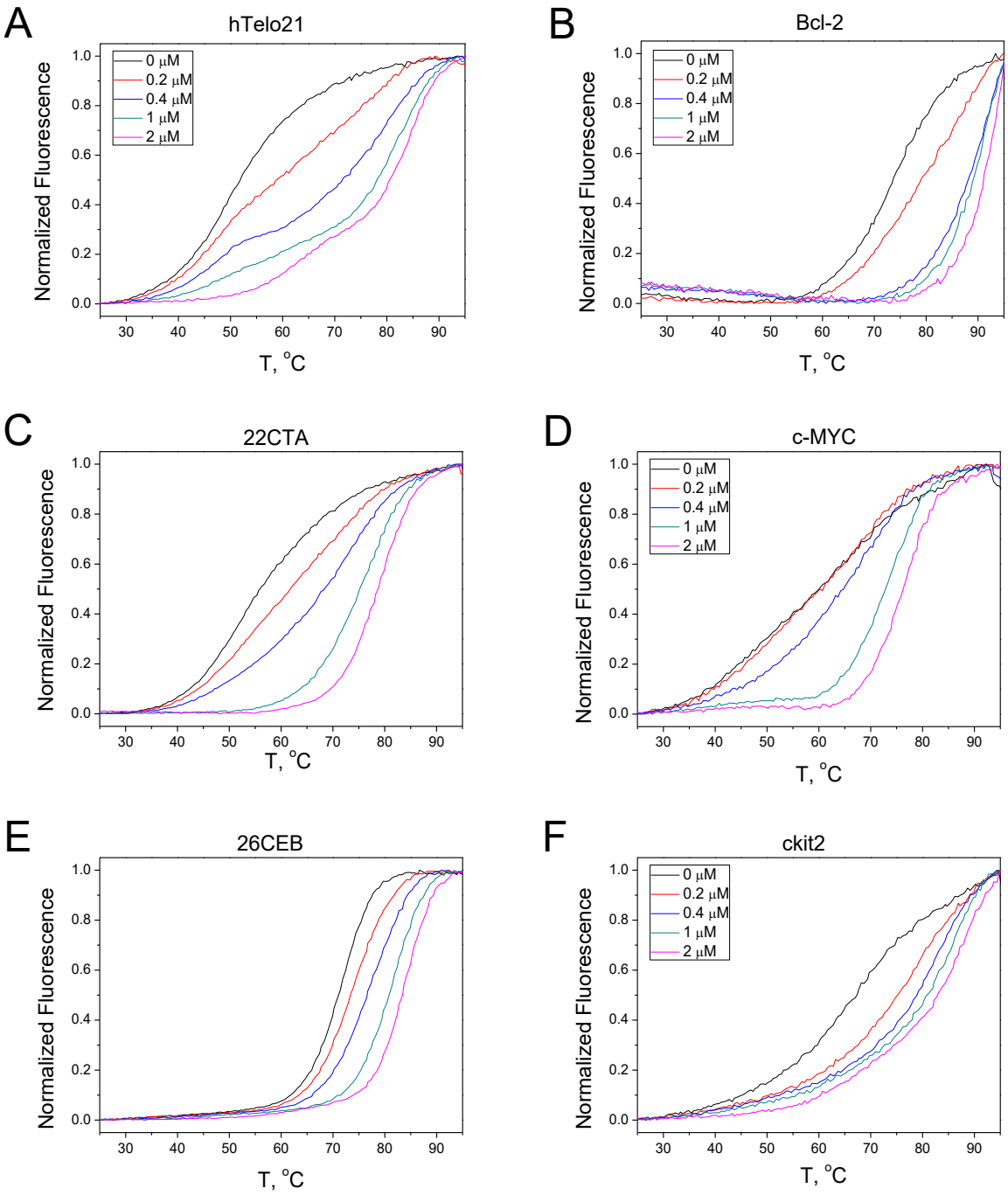
A
hTelo21
B
Bcl-2
C
22CTA
D
c-MYC
E
26CEB
F
ckit2
0 μM
0.2 μM
0.4 μM
1 μM
2 μM
Normalized Fluorescence
T, °C

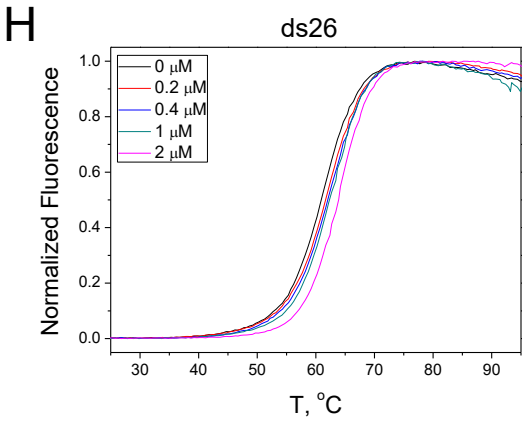

Figure S18. FRET melting assay F-HTelo21-T (**A**), F-Bcl-2-T (**B**), F-22CTA-T (**C**), F-c-MYC--T (**D**), F-26CEB-T (**E**), F-ckit2-T (**F**), ds26 (**H**) with increasing concentration of **1** (0-2 μM).

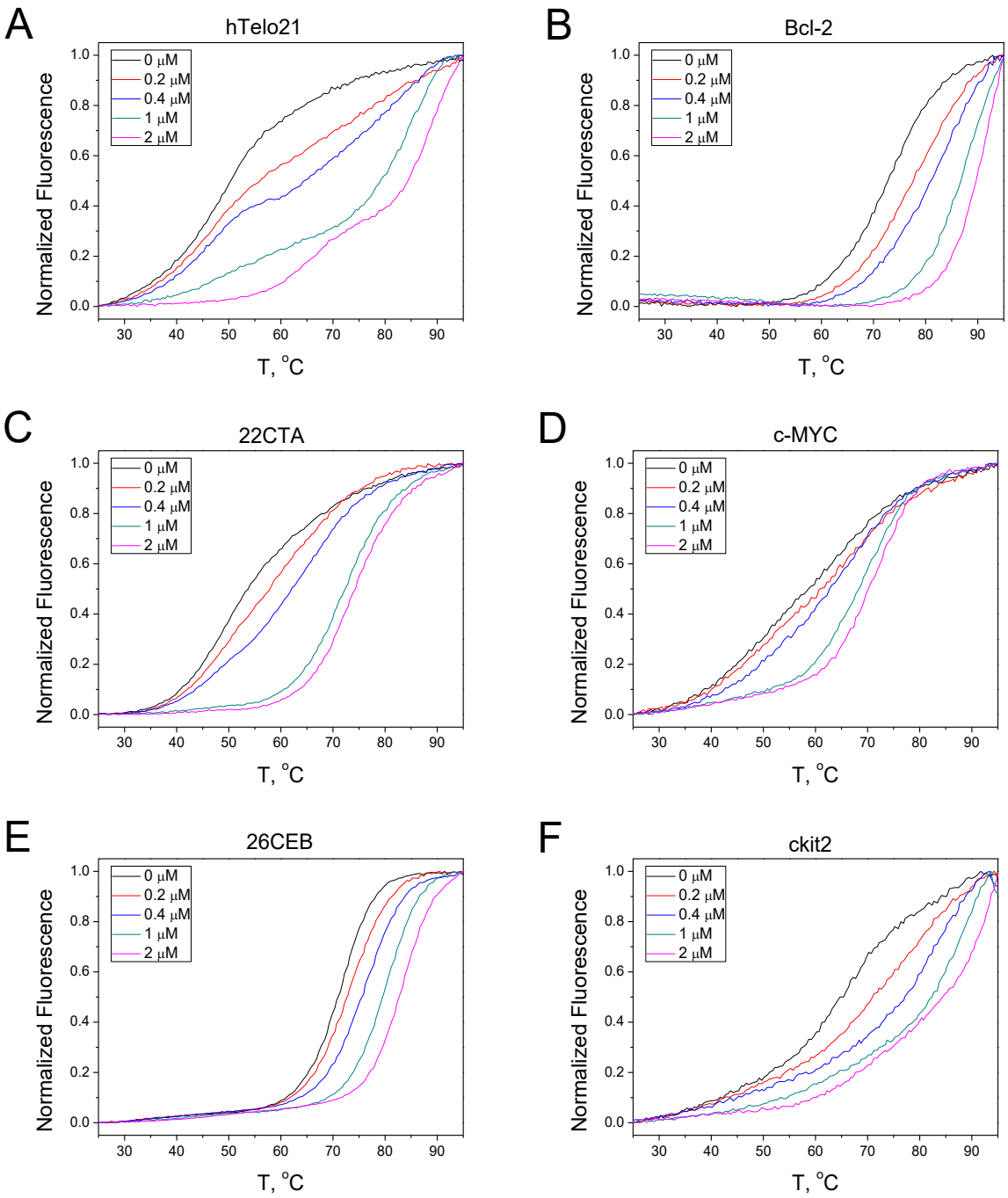
A
hTelo21
B
Bcl-2
C
22CTA
D
c-MYC
E
26CEB
F
ckit2
0 μM
0.2 μM
0.4 μM
1 μM
2 μM
Normalized Fluorescence
T, °C

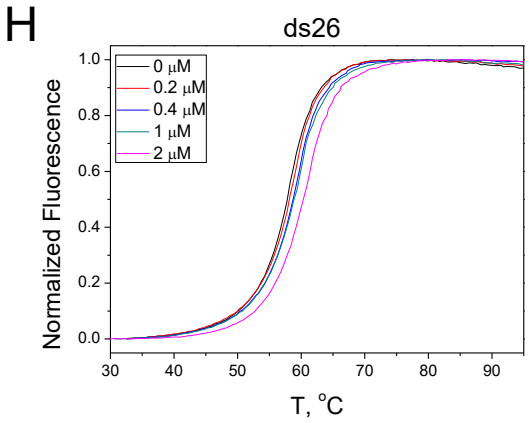

Figure S19. FRET melting assay F-HTelo21-T (**A**), F-Bcl-2-T (**B**), F-22CTA-T (**C**), F-c-MYC--T (**D**), F-26CEB-T (**E**), F-ckit2-T (**F**), ds26 (**H**) with increasing concentration of **2** (0-2 μM).

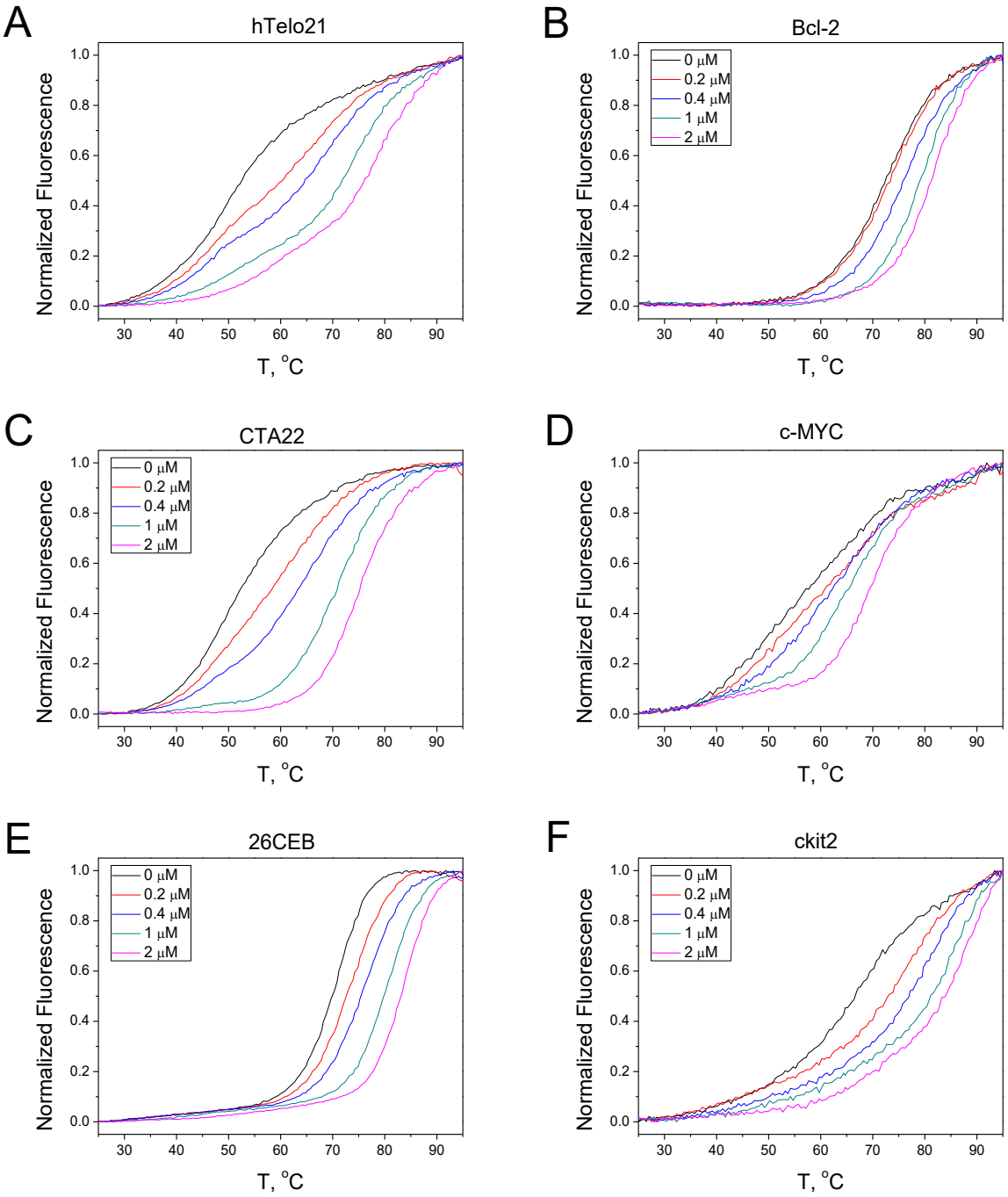
A
hTelo21
B
Bcl-2
C
CTA22
D
c-MYC
E
26CEB
F
ckit2
Normalized Fluorescence
T, °C
0 μM
0.2 μM
0.4 μM
1 μM
2 μM

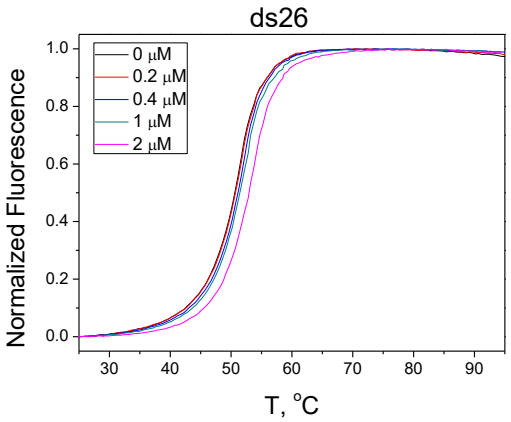

Figure S20. FRET melting assay F-HTelo21-T (**A**), F-Bcl-2-T (**B**), F-22CTA-T (**C**), F-c-MYC--T (**D**), F-26CEB-T (**E**), F-ckit2-T (**F**), ds26 (**H**) with increasing concentration of **3** (0-2 μM).

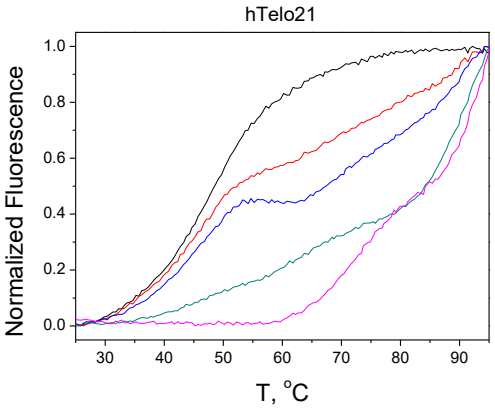
hTelo21
Normalized Fluorescence
T, °C

B

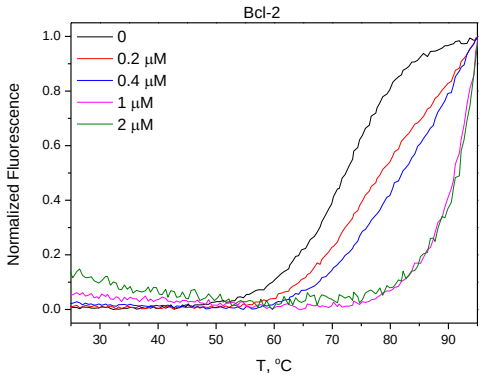
Bcl-2
0
0.2 μM
0.4 μM
1 μM
2 μM
Normalized Fluorescence
T, °C

C

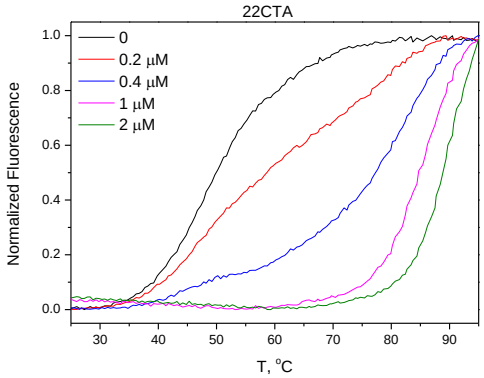
22CTA
0
0.2 μM
0.4 μM
1 μM
2 μM
Normalized Fluorescence
T, °C

D

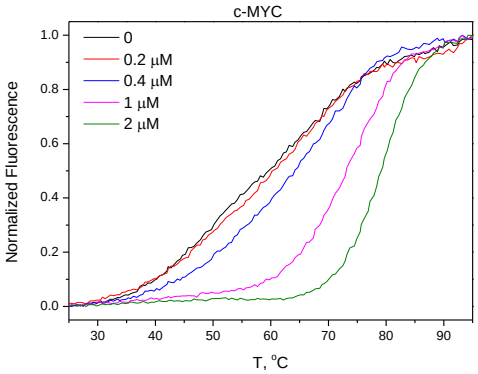
c-MYC
0
0.2 μM
0.4 μM
1 μM
2 μM
Normalized Fluorescence
T, °C

E

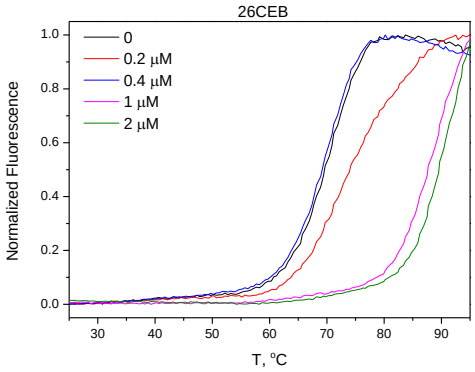
26CEB
0
0.2 μM
0.4 μM
1 μM
2 μM
Normalized Fluorescence
T, °C

F

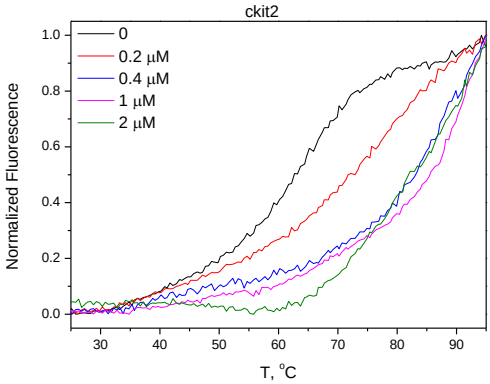
ckit2
0
0.2 μM
0.4 μM
1 μM
2 μM
Normalized Fluorescence
T, °C

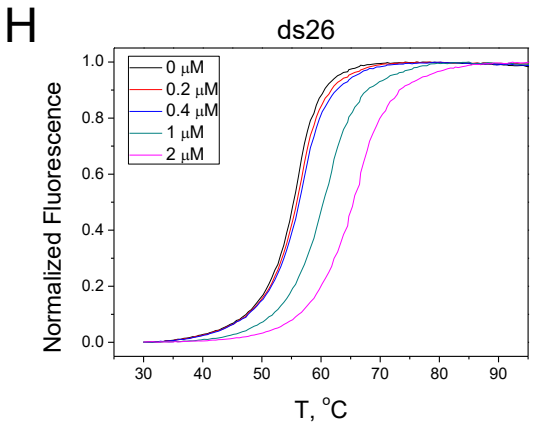

Figure S21. FRET melting assay F-HTelo21-T (**A**), F-Bcl-2-T (**B**), F-22CTA-T (**C**), F-c-MYC-T (**D**), F-26CEB-T (**E**), F-ckit2-T (**F**), ds26 (**H**) with increasing concentration of **4** (0-2 μM).

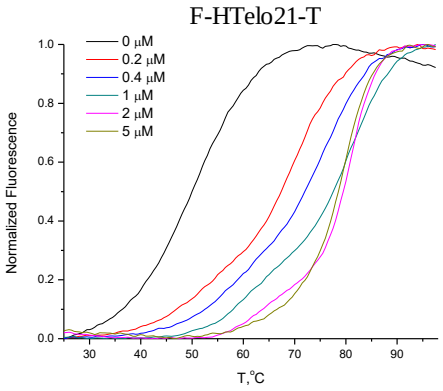
F-HTelo21-T
0 μM
0.2 μM
0.4 μM
1 μM
2 μM
5 μM
Normalized Fluorescence
T,°C

A

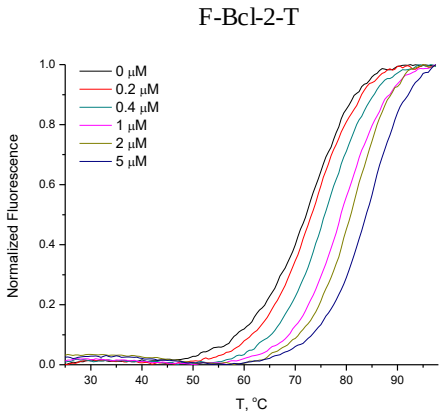
F-Bcl-2-T
0 μM
0.2 μM
0.4 μM
1 μM
2 μM
5 μM
Normalized Fluorescence
T, °C

B

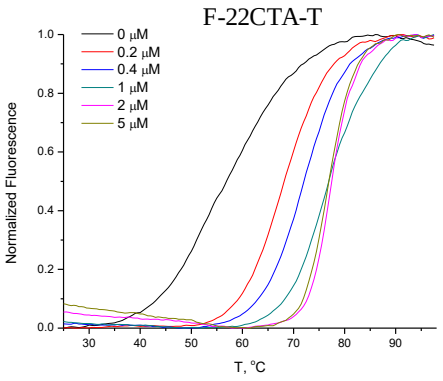
F-22CTA-T
0 μM
0.2 μM
0.4 μM
1 μM
2 μM
5 μM
Normalized Fluorescence
T, °C

C

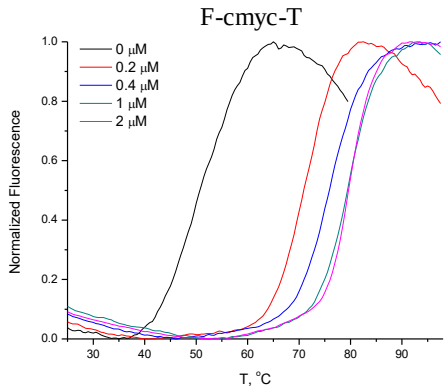
F-cmyc-T
0 μM
0.2 μM
0.4 μM
1 μM
2 μM
Normalized Fluorescence
T, °C

D

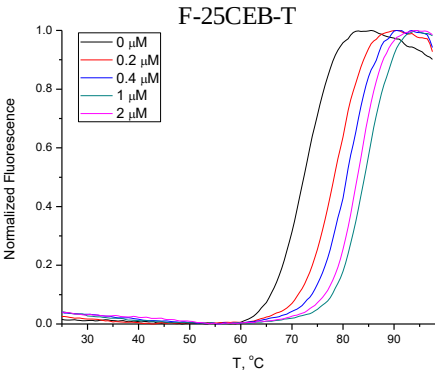
F-25CEB-T
0 μM
0.2 μM
0.4 μM
1 μM
2 μM
Normalized Fluorescence
T, °C

E

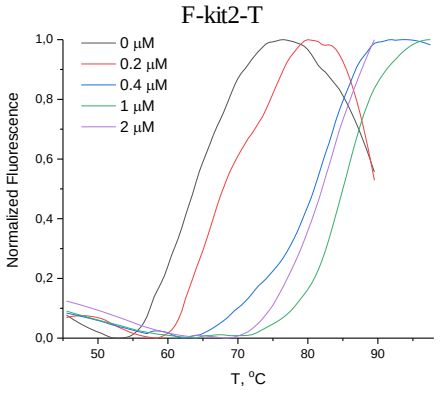
F-kit2-T
0 μM
0.2 μM
0.4 μM
1 μM
2 μM
Normalized Fluorescence
T, °C

F

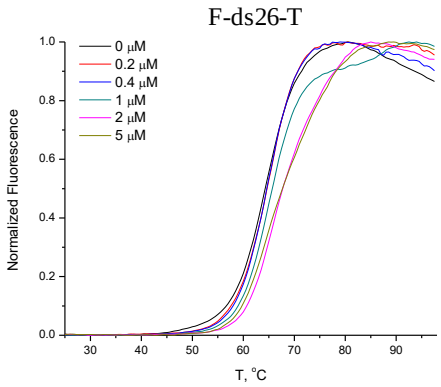

H

Figure S22. FRET melting assay F-HTelo22-T (**A**), F-Bcl-2-T (**B**), F-22CTA-T (**C**), F-c-MYC--T (**D**), F-26CEB-T (**E**), F-ckit2-T (**F**), ds26 (**H**) with increasing concentration of **5** (0-2 μM).

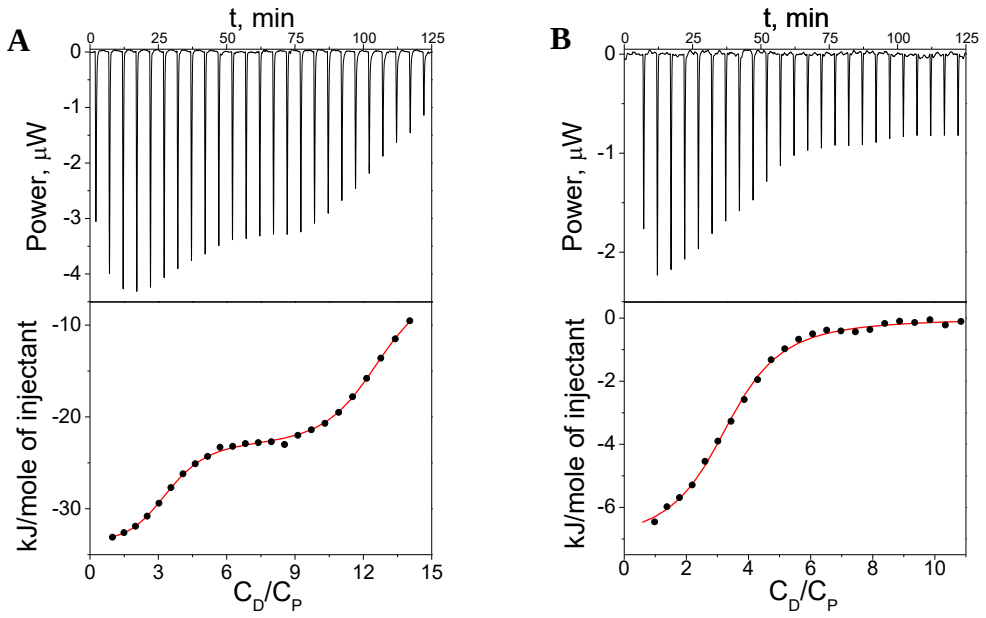

Figure S23. ITC titration of the **2**/HTelo22 system (**A**) and of the **3**/HTelo22 system (**B**). [complex] = 1 mM.

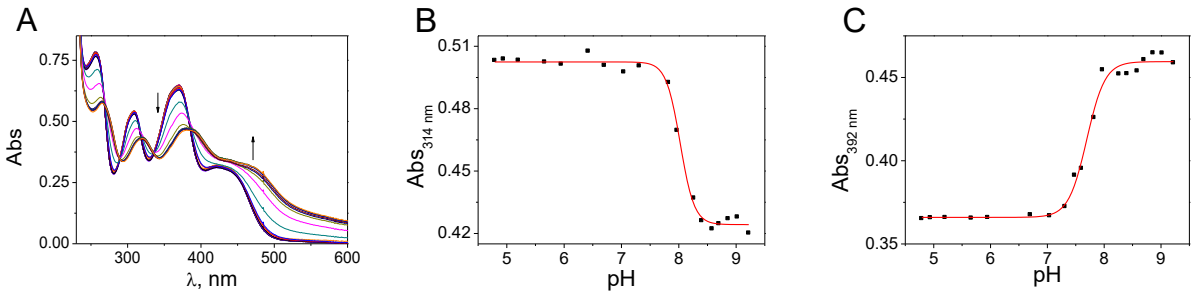

Figure S24. A) Absorbance spectra of **1** recorded with increasing pH (arrow sense) from pH = 4.5 to pH = 9.5. **B)** Absorbance Vs pH plot of **1** at λ = 314 nm and **C)** λ = 392 nm.

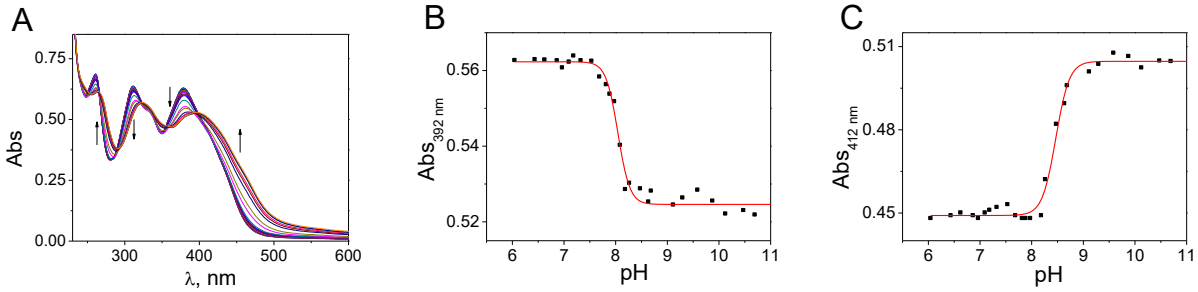

Figure S25. A) Absorbance spectra of **2** recorded with increasing pH (arrow sense) from pH = 4.5 to pH = 11. **B)** Absorbance Vs pH plot of **2** at λ = 392 nm and **C)** λ = 412 nm.

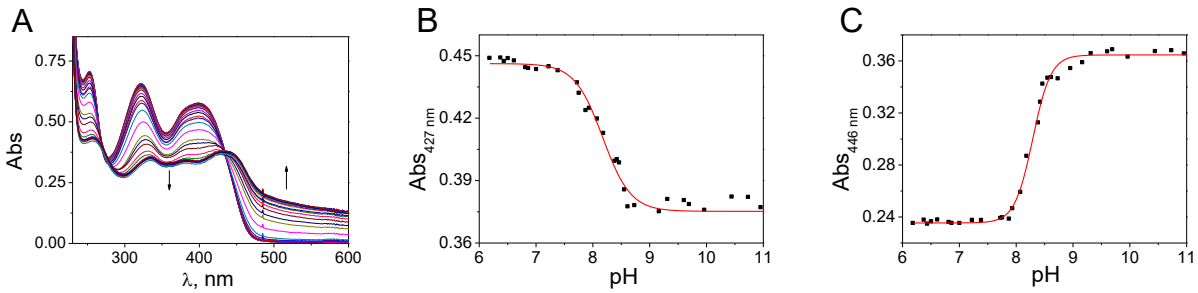

Figure S26. A) Absorbance spectra of **3** recorded with increasing pH (arrow sense) from pH = 4.5 to pH = 11. **B)** Absorbance Vs pH plot of **3** at λ = 427 nm and **C)** λ = 446 nm.

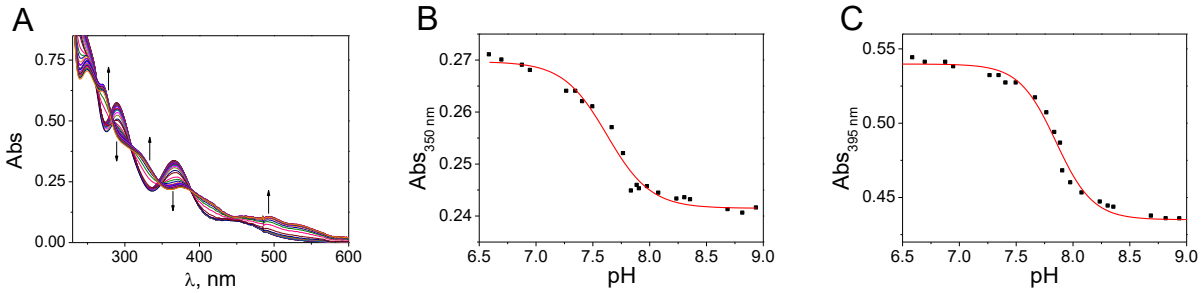

Figure S27. A) Absorbance spectra of **4** recorded with increasing pH (arrow sense) from pH = 4.5 to pH = 11. **B)** Absorbance Vs pH plot of **4** at λ = 350 nm and **C)** λ = 395 nm.

Table S2. pKa_1 and pKa_2 values obtained for **1**-**4**.

Compound	pKa_1	pKa_2
1	7.69 ± 0.02	8.02 ± 0.01
2	8.04 ± 0.02	8.47 ± 0.02
3	8.17 ± 0.03	8.30 ± 0.01
4	7.62 ± 0.02	7.85 ± 0.01

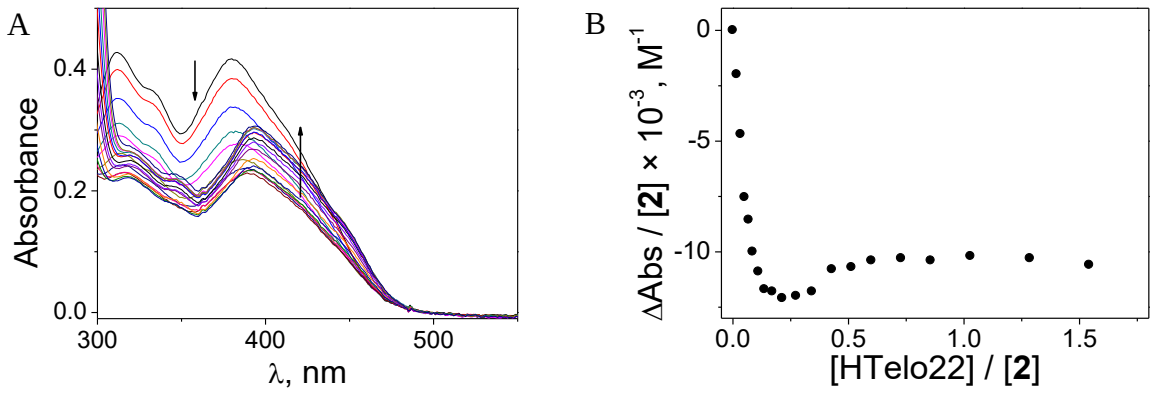

Figure S28. A) Absorbance spectra of the UV-Vis titration of HTelo22 and **2** ([**2**] = 20 μM). B) Absorbance binding isotherm of **2** with increasing amounts of HTelo22 at λ = 380 nm.

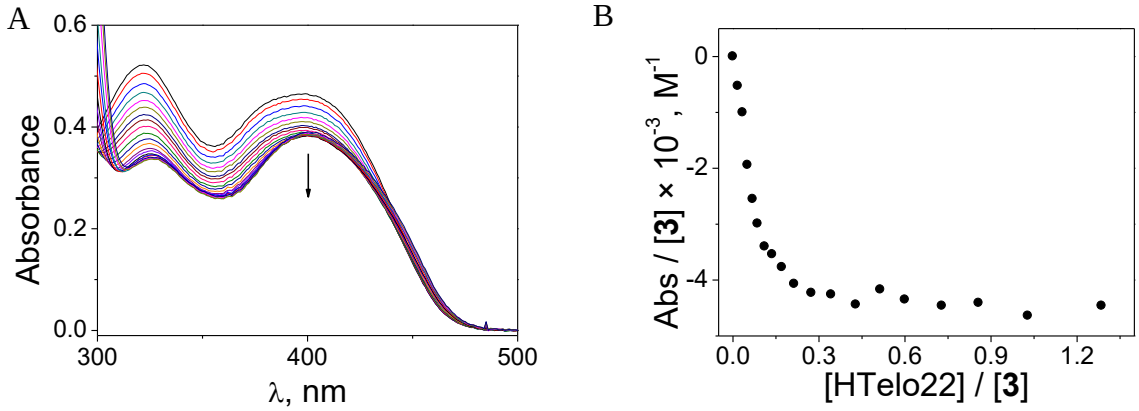

Figure S29. A) Absorbance spectra of the UV-Vis titration of HTelo22 and **3** ([**3**] = 20 μM). B) Absorbance binding isotherm of **3** with increasing amounts of HTelo22 at λ = 400 nm.

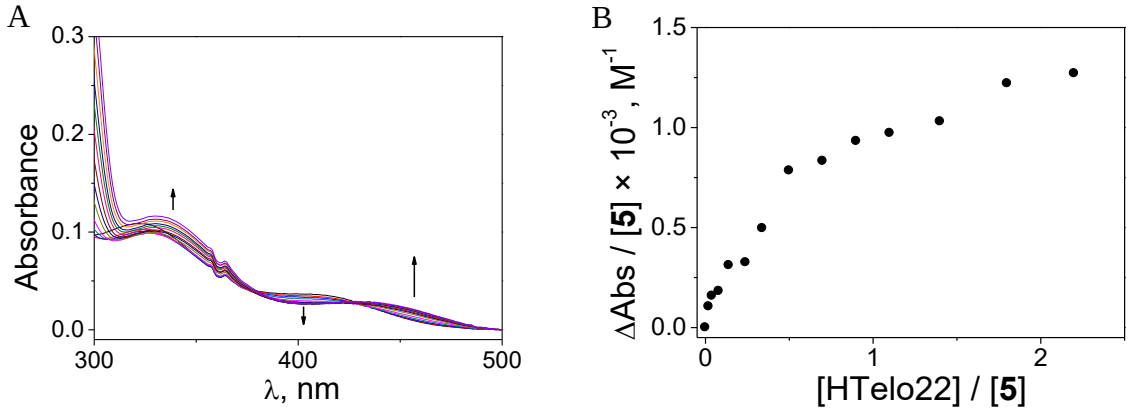

Figure S30. A) Absorbance spectra of the UV-Vis titration of HTelo22 and **5** ([**5**] = 20 μM). B) Absorbance binding isotherm of **5** with increasing amounts of HTelo22 at λ = 450 nm at λ = 450 nm).

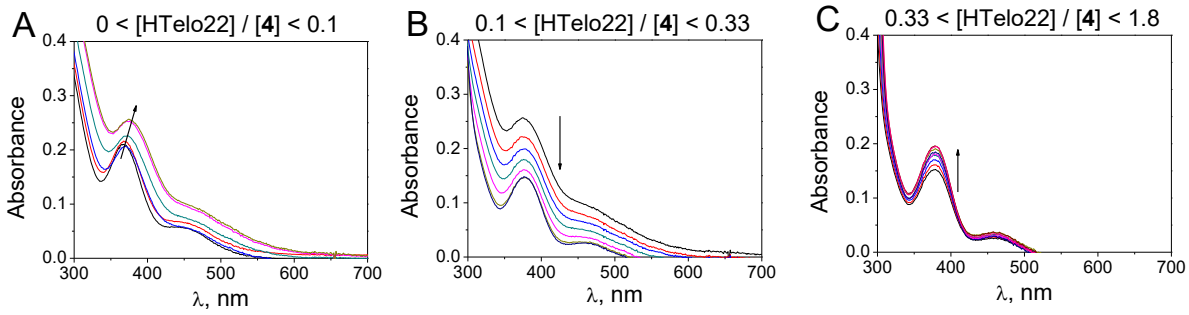

Figure S31. Absorbance spectra of the **4**/HTelo22 system recorded during titration at $0 \leq$ [HTelo22]/[**4**] ≤ 0.1 (**A**), $0.1 \leq$ [HTelo22]/[**4**] ≤ 0.33 (**B**) and $0.33 \leq$ [HTelo22]/[**4**] ≤ 1.8 (**C**). [complex] = 20 μM.

Absorption titration studies

For absorbance binding measurement of the complexes with HTelo22 DNA, 10 μM of the complex was titrated with concentrated solutions of DNA in 50 mM Tris-HCl buffer (pH 7.) with 10 mM KCl. Absorbance spectra were recorded 2 minutes after each addition of concentrated DNA solution, in order to allow complete stabilization of the complex and oligonucleotide until absorbance saturation was reached. A 1 cm path-length quartz cuvette was used to carry out the measurements.

Binding constants were obtained according to the independent-site model by nonlinear fitting to equation 2 (see: F.H. Stootman et al. *Analyst*, **2006**, *131*, 1145-1151)

$$\Delta Abs_{obs} = \varepsilon\Delta_{[HG]} * [HG] \qquad \textbf{Equation 1}$$

and

$$[HG] = \frac{1}{2}\left([G]_0 + [H]_0 + \frac{1}{K_a}\right) - \sqrt{\left([G]_0 + [H]_0 + \frac{1}{K_a}\right)^2 - 4[H]_0[G]_0} \qquad \textbf{Equation 2}$$

where Abs = absorbance intensity, $[H]_0$ = initial host concentration (compound), $[G]_0$ =initial guest concentration (i.e. DNA), [HG] = host − guest concentration, Ka =affinity constant, $\epsilon\Delta_{[HG]}$ = molar extinction coefficient of host − guest species. The parameters were found via the Levenberg−Marquardt fitting routine in Origin 8.5 software.

Table S3. Binding constants (K_a, in triplicate) and spectroscopic properties of complexes calculated from UV/Vis titrations of complexes with HTelo22 (50 mM Tris-HCl, 10 mM KCl, pH 7.0, T = 25 ºC).

Compound	Change in intensity of λ_{max}	Shift λ_{max}	K_a (M^{-1})
1	40 %	369 to 381	n.d.
	-43 %	none	
2	51 %	380 to 393	n.d.
	-28 %	none	
3	37 %	322 to 325	9.4 (± 0.7) x 10^4
4	-21 %	367 to 374	n.d.
	35 %	374 to 377	
	-31 %	377 to 379	
5	-17 %	none	1.3 (± 0.4) x 10^5

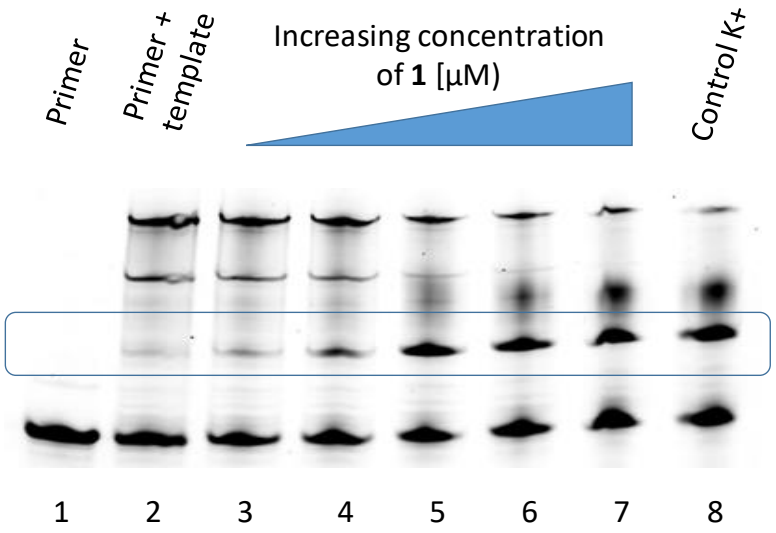

Figure S32. Polymerase Stop Assay (PSA) with a template strand containing the G4-forming sequence from the *c-Myc* gene promoter. (A) Image of the polyacrylamide gel electrophoresis showing the control lanes (1, 2 and 8) as well as the effect of increasing concentration of compound **1** (0.3, 1, 5, 10 and 20 µM) on the product distribution (lanes 3-7).

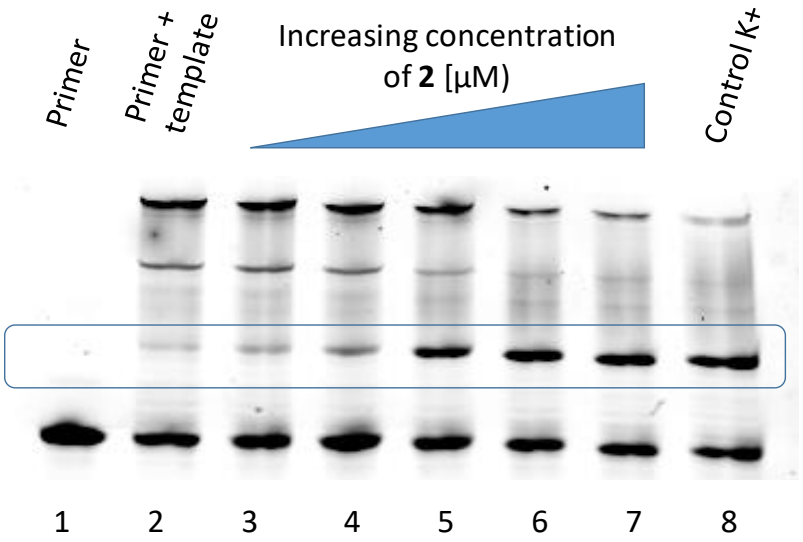

Figure S33. Polymerase Stop Assay (PSA) with a template strand containing the G4-forming sequence from the *c-Myc* gene promoter. (A) Image of the polyacrylamide gel electrophoresis showing the control lanes (1, 2 and 8) as well as the effect of increasing concentration of compound **2** (0.3, 1, 5, 10 and 20 µM) on the product distribution (lanes 3-7).

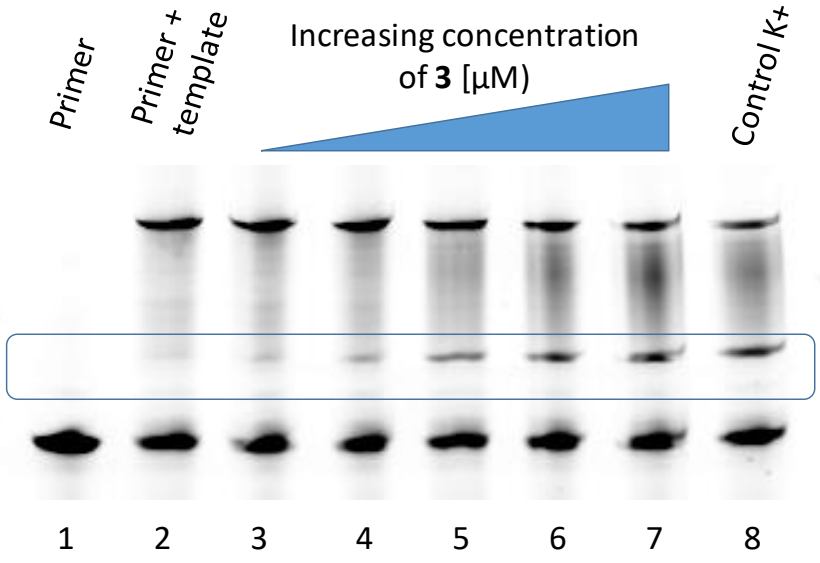

Figure S34. Polymerase Stop Assay (PSA) with a template strand containing the G4-forming sequence from the *c-Myc* gene promoter. (A) Image of the polyacrylamide gel electrophoresis showing the control lanes (1, 2 and 8) as well as the effect of increasing concentration of compound **3** (0.3, 1, 5, 10 and 20 µM) on the product distribution (lanes 3-7).